Journal of Materials Chemistry A

Materials for energy and sustainability

Accepted Manuscript

This article can be cited before page numbers have been issued, to do this please use: M. Devi, J. Shikhar and S. Sharma, *J. Mater. Chem. A*, 2025, DOI: 10.1039/D5TA06469D.



This is an Accepted Manuscript, which has been through the Royal Society of Chemistry peer review process and has been accepted for publication.

Accepted Manuscripts are published online shortly after acceptance, before technical editing, formatting and proof reading. Using this free service, authors can make their results available to the community, in citable form, before we publish the edited article. We will replace this Accepted Manuscript with the edited and formatted Advance Article as soon as it is available.

You can find more information about Accepted Manuscripts in the <u>Information for Authors</u>.

Please note that technical editing may introduce minor changes to the text and/or graphics, which may alter content. The journal's standard <u>Terms & Conditions</u> and the <u>Ethical guidelines</u> still apply. In no event shall the Royal Society of Chemistry be held responsible for any errors or omissions in this Accepted Manuscript or any consequences arising from the use of any information it contains.



Effect of nitrogen content on performance of supercapacitors composed of nitrogen-carbon materials

Mamta Devi ^{1†}, Jyoti Shikhar^{1†}, and Swati Sharma^{1*}

¹School of Mechanical and Materials Engineering, Indian Institute of Technology Mandi, Kamand, HP, 175075, India

E-mail: swati@iitmandi.ac.in

[†] Equally contributing authors

Abstract

Nitrogen-carbon (N-C) materials are emerging as strong contenders to elemental carbon in advanced energy applications. Here we have established a correlation between the nitrogen content and supercapacitor performance in N-C materials. The core concept is that the functionalities of such materials are strongly influenced by the fraction, distribution and chemical configuration of nitrogen in the carbon network. The investigation is carried out on a graphitic carbon nitride (g-CN), from which nitrogen is gradually removed to produce N-C materials having N/C ratios between 0.52 to 0.10. Material with a N/C of 0.15 exhibits the highest capacitance, achieving 79.25 ± 3.8 F/g (volumetric capacitance of 1585 F/cm³) at a current density of 1 A/g. These findings are particularly relevant to g-CN-derived disordered and non-graphitizing carbon systems but are also applicable to other forms of carbon. Precisely tuning the nitrogen content can guide targeted material synthesis and enable first-principles evaluation of an N-C material's suitability for supercapacitor applications.

Introduction

The functionalities of carbon materials in energy applications can be enhanced manifold by incorporating a heteroatom such as nitrogen (N) into the carbon network ^{1–3}. For crystalline carbons such as diamond and graphite, N can be incorporated in a controlled manner, and its lone electron pair can be precisely used for well-defined applications such as magnetic field sensing ^{4,5}. The same does not hold true for disordered carbons. The fraction, position, distribution and even characterization of N atoms in disordered carbon are difficult to achieve accurately ^{6,7}. This is primarily because such carbon materials are often complex nongraphitizing systems, which feature variable extents of graphitic content ⁸. Small graphitic crystallites having turbostratic carbon layers, typically with five- and seven-membered rings are distributed within such materials, along with 5-7% fullerenes incorporated in them ⁹. Consequently, while many examples of the use of non-graphitizing carbons containing N in both battery and supercapacitor devices have been reported ^{10–12}, and different morphologies ¹³, pore sizes ^{14,15}, naturally abundant precursors ^{15,16}, and composites ^{17,18} have been explored, the exact mechanism and the influence of the fraction of N for energy storage systems of N-containing carbons remain largely unexplored.

The fraction of nitrogen in N-C materials is known to be strongly intertwined with their crystallinity⁸. The highest ratio of N to C that would yield a stable compound is 4/3, which is the case in stoichiometrically balanced graphitic carbon nitride (g-C₃N₄)¹⁹ 20. The lowest N-content is zero, that of pure carbon. Between these two extremes, an entire range of disordered N-C materials exist. They are the ones of interest in energy applications, as the presence of N in the carbon network locally changes the polarity of the carbon molecules (rings or sheets)^{21,22}. These slightly polarized regions serve as active sites that improve electron transfer reactions with the electrolyte. However, simply increasing the N fraction does not always lead to an improved electrochemical performance, as there is a trade-off between electrical conductivity and the number of polarized active sites in the material. In addition to the N/C ratio, these two properties depend upon the structural configuration(s)

Open Access Article. Published on 05 Novemba 2025. Downloaded on 11/11/2025 06:10:41.

This article is licensed under a Creative Commons Attribution-NonCommercial 3.0 Unported Licence.

adopted by the N atoms in the carbon network, *i.e.*, whether N is present as pyrollic, pyridinic and graphitic forms $^{23-25}$. In various studies it has been suggested that pyridine N has the highest impact on the pseudocapacitive energy storage mechanism exhibited by the presence of N in a carbon system 21,26,27 .

N-containing carbon systems are commonly achieved via three pathways, (i) in-situ incorporation during the synthesis of the carbon material, (ii) ex-situ incorporation, i.e., after the synthesis of the carbon material, and (iii) thermal de-nitrogenation of g-CN²⁸29. The first two methods yield N-containing carbons with a low N/C ratio (N/C \leq 0.10) and offer less control on the configuration of N in the material. These materials generally contain pyrrolic, pyridinic and graphitic nitrogen species along with surface functional groups such as amines and amides³⁰. The supercapacitor performance of such N-C systems with low N/C ratios has been widely investigated ^{31–33}. It is suggested that N–C materials with a high proportion of pyridinic and pyrrolic nitrogen species contribute significantly to pseudocapacitance (a combination of reversible faradic reactions with Electrical Double Layer type capacitance³⁴. The third pathway involving the thermal de-nitrogenation of g-CN offers greater control over the nitrogen configuration in the resulting N-C materials. This method typically produces materials rich in pyridinic and graphitic nitrogen, with N/C ratios ranging from that of the g-CN precursor (1.33–0.35) down to as low as 0.01, depending upon the temperatures used in the process ≥ 2500 °C. In all aforementioned cases, individual N-C materials have been evaluated for their supercapacitor performance, without establishing any correlation with their N/C ratio, which is indeed the key player in their electrochemical activity. By and large, the following questions remain unanswered: (i) how the ratio of N/C in such materials influences the supercapacitor performance, (ii) what is the exact storage mechanism of such supercapacitors, and whether it is the same in all N-C materials, and finally, (iii) what is the optimum N/C ratio for a device fabrication.

To study the effect of the N-content on supercapacitor performance of N-C materials featuring $0.10 \le N/C \le 1$, we prepared four different N-C materials exhibiting different

N/C ratios in the following steps: (i) autoclave-assisted solvent-free heat-treatment of urea and citric acid to generate a g-CN material with a N/C ratio of 0.52, which is the first N-C material of investigation (ii) further heat-treatment of this g-CN in a tube furnace at different target temperatures to methodically eliminate nitrogen and derive three materials with N/C ratio of 0.32, 0.15 and 0.10, respectively, and (iii) electrode preparation using these four materials for supercapacitor studies. These four N/C samples were characterized for their supercapacitor performance via cyclic voltammetry (CV), galvanostatic chargedischarge tests (GCD), electrochemical impedance spectroscopy (EIS) and long term stability tests for 2500 GCD cycles.

Materials and Methods

Materials

Urea (> 99 %) and citric acid (>99 %) were procured from Qualigens, India and Sigma-Aldrich USA, respectively. Centrifuge: 5810 R (Eppendorf, India), Lindberg blue M furnace (Thermo Scientific, TF55035C-1, USA) and Planetary ball mill (Retsch PM-100, Germany,) were used for centrifuge, heat-treatment, and ball milling processes respectively.

Methods

Citric acid and urea, in a molar ratio of 1:6, were placed in a Teflon-lined autoclave (commonly referred to as a hydrothermal reactor) and heated at 200 °C for 1 hour. After cooling, the resulting mixture was dissolved in ethanol and subjected to sonication for 6 hours. This was followed by centrifugation at 2500 rpm for 10 minutes. The supernatant was used for a different study, and the solid residue was collected for further processing. The residue was thoroughly washed multiple times with ethanol and then air-dried at 80 °C for 6 hours to obtain the bulk graphitic carbon nitride (g-CN) material, designated as N-C₂ (where 2 denotes its preparation temperature /100) and featured a N/C ratio of 0.52.

Open Access Article. Published on 05 Novemba 2025. Downloaded on 11/11/2025 06:10:41

N-C₂ was subsequently subjected to thermal treatment in a Lindberg Blue furnace. The sample was heated from room temperature to 600 °C at a ramp rate of 10 °C/min, with a dwell time of 1 hour, under a continuous nitrogen flow of 200 SCCM to ensure an inert atmosphere. The material obtained after this process was labeled as N-C₆ with a N/C ratio of 0.32. Similarly, heat treatments were conducted at 900 °C and 1300 °C under identical conditions to yield materials labelled as N-C₉ and N-C₁₃ with N/C ratio of 0.15 and 0.10 respectively, where the numeric designation corresponds to the hundredth digit of the treatment temperature.

Each material, N-C₂, N-C₆, N-C₉ and N-C₁₃ was transferred into a 50 mL tungsten carbide jar containing ten 10 mm tungsten carbide balls. Wet ball milling was performed at 300 rpm for 3 hours (using 50 minutes milling followed by 10 minutes rest cycles). The weight ratio of milling balls to N-C material to ethanol was maintained at 20:2:1. The resulting ball-milled N-C materials were subsequently used in electrode fabrication for electrochemical studies.

Material characterizations

X-ray diffraction (XRD) of the N-C powder materials were performed on SmartLab 9kW rotating anode X-ray diffractometer (Rigaku Corporation) having a monochromatic Cu K α radiation (1.54 Å) source. Samples were scanned over the range of 2θ , 5-90 °, with a scan rate of 3 °/min. The diffraction pattern was analyzed by Rietveld refinement using X'pert Highscore Plus software. The values of interlayer spacing (d) were calculated using Bragg's diffraction law. Raman spectra of the N-C materials were recorded on the HORIBA LabRAM Jobin Vyon spectrometer with a 20 mW air-cooled argon laser (532 nm) for excitation. The spectra were recorded from 300 to 3500 cm⁻¹ spectral range using an ultralow frequency filter, 1800 grooves/mm grating, and Peltier cooled CCD for 150 s acquisition time. X-Ray photoelectron spectroscopy (XPS) spectra of the N-C materials were recorded on Nexsa base (Thermofisher scientific) surface analysis with a micro-focused (400 μ m, 72 W, 12000 V) monochromatic Al-K α source (h $\nu = 1486.6$ eV, wavelength = 0.83 nm). The XPS survey scan spectra were recorded from 0 to 1350 eV binding energy. Data were collected at a pass energy of 40 eV with a step size of 0.1 eV. The narrow scan spectra of all the components were deconvoluted using XPS Peak41 curve-fitting software and Gaussian fit was used for peak fitting. A modified Shirley background, which includes additional constraints to ensure that the background intensity remains lower than the actual data at any point within the region, was employed for deconvolution. Adventitious carbon at 284.8 eV was used as the reference point. The nitrogen gas adsorption-desorption isotherms at 77 K for the N-C powder materials were recorded on a Quanta chrome Autosorb-iQ-MP/XR137 system to assess the Brunauer-Emmett-Teller (BET) surface area. Contact angle measurements of the pelletized N-C materials were done on SEO Phoenix 300 Touch Contact Angle at Room temperature and DI water droplets (15 μ L volume) were used for measuring the contact angle. The electrical characterization of the pelletized N-C materials were performed using a KEITHLEY 4200 SCS system connected to a cascade probe station equipped with $\sim 20~\mu m$ Ti probes. The voltage measurements were conducted using the four-point probe method, with a current range of -10 μ A to 10 μ A. The sheet resistance was calculated from the I-V data using the van der Pauw method. Elemental analysis of N-C powder materials were carried out using the B100003212 UNIQUBE system for simultaneous CHNS analysis, with the capability for oxygen determination via a thermal conductivity detector (TCD).

Electrochemical measurements

All the electrochemical measurements were performed in 1 M Na₂SO₄ electrolyte solution using a Biologic EC lab (SP-300) instrument. Platinum (Pt) wire and Ag/AgCl were employed as the counter and reference electrodes, respectively. At first, the ball milled N-C material, carbon black and polyvinylidene fluoride (PVDF) were mixed in a ratio of 8:1:1 with N-Methyl-2-pyrrolidone (NMP) solvent. The prepared slurry was then coated on a carbon cloth (area: $1 \times 1 \text{ cm}^2$; thickness: 0.5 mm) using a doctor blade, with mass of the

Open Access Article. Published on 05 Novemba 2025. Downloaded on 11/11/2025 06:10:41

active material as 10 mg cm⁻². The coated sheet was dried at 80 °C for 12 hr in a hot air oven and used as the working electrode. Electrochemical impedance spectroscopy (EIS) measurements were performed in the frequency range of 1 MHz to 0.1 Hz at 500 mV to investigate the resistive and capacitive behaviour of the N-C samples.

Results and Discussions

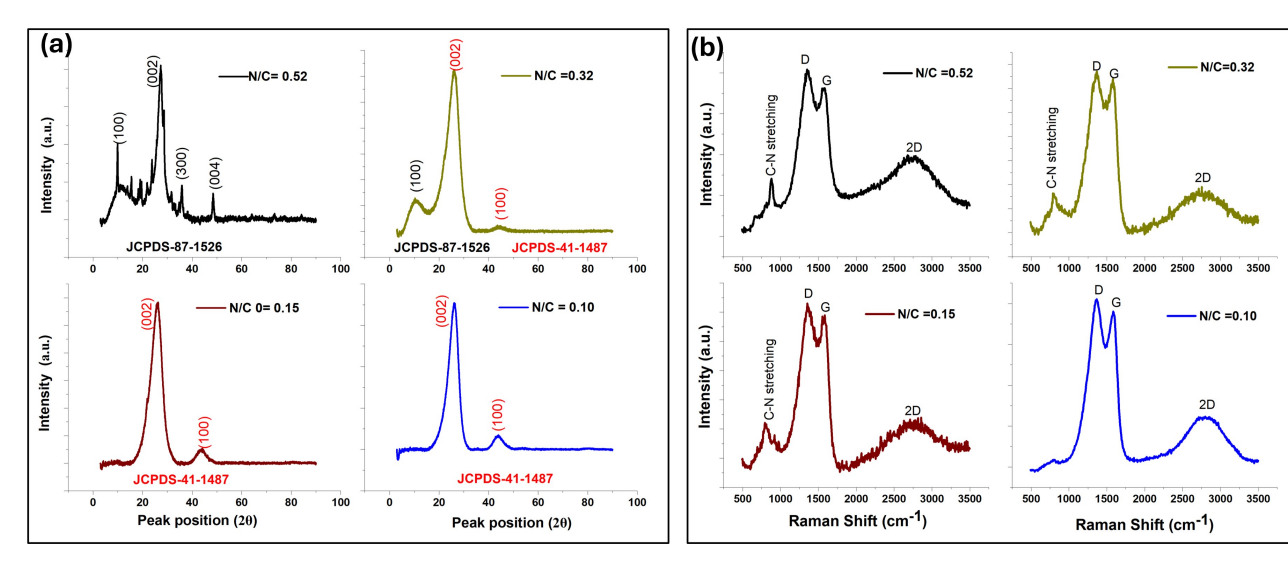


Figure 1: (a)XRD plots, and (b) Raman spectra of N-C materials with N/C ratio of 0.52, 0.32, 0.15 and 0.10.

Results of the microstructure analysis of all four N-C materials evaluated via XRD and Raman spectroscopy are provided in Figure 1a)(Figure 1b respectively. A summary of the characterization of these N-C materials is provided in Table 1. The XRD peaks were fitted using JCPDS-87-1526 (hexagonal g-CN) for N/C = 0.52; both JCPDS-87-1526 and JCPDS-41-1487 (hexagonal graphite) for N/C = 0.32; and JCPDS-41-1487 alone for N/C = 0.15 and 0.10. The XR-diffractograms (refer to Figure 3a) of the N-C material with an N/C ratio of 0.52 reveals the presence of crystalline graphitic carbon nitride (g-CN) phases, as indicated by diffraction peaks at 12°, 27.2°, 34.8° and 48.9° corresponding to the (100), (002), (300), and (004) planes of g-CN, respectively. These findings are consistent with previous reports⁸. For the sample with an N/C ratio of 0.32, diffraction peaks from both

g-CN and graphitic carbon phases are observed. The peak at 12° is attributed to the (100) plane of g-CN, while peaks at 24.8° and 43.2° correspond to the (002) and (100) planes of graphitic carbon, respectively. In the materials with N/C ratios of 0.15 and 0.10, the diffraction peaks at 24.9° and 43.4° arising from the (002) and (100) planes, confirm the presence of graphitic but disordered carbon phases. Interlayer spacing values for these N-C materials are listed in Table 1. Raman spectra (refer to Figure 3b) of the N-C samples show features characteristic of disordered carbon, with distinct D, G and 2D bands observed at 1340, 1578, and 2780 cm⁻¹, respectively. Furthermore, the presence of a peak at 810 cm⁻¹, corresponding to the C-N stretching mode, in the spectra of materials with N/C ratios of 0.52, 0.32, and 0.15, confirms the incorporation of nitrogen into the structure. These results are in agreement with previous studies on similar materials 35,36 . The I_D/I_G ratio and the coherence length (L_a, nm) $^{37-39}$, calculated using the formula given in Equation 1, where λ is the laser wavelength of 532 nm, are the two indexes that reveal the crystallinity in the (10) planes of the N-C materials. The values of these two indexes are provided in Table 1, which confirm that the crystallinity in the (10) planes decrease initially and then further increase with decreasing N/C ratio.

$$L_a = (2.4 \times 10^{-10}) \times (\lambda^4) \times \frac{I_G}{I_D}$$
 (1)

TEM images and SAED pattern of N-C material at N/C = 0.52 (see Figure 2a and b), reveal a disordered g-CN material with percolated crystalline regions. At N/C = 0.32, the N-C material converts into a turbostratic graphitic material with high degree of disorder (see Figure 2c and d). At N/C = 0.15, the disorder in the N-C material reduces as evident from the more graphitic regions in the TEM image and prominent rings in the SAED pattern (see Figure 2e and f) and with further decrease in N/C ratio, at N/C = 0.10, more graphitic regions and prominent diffraction rings in the SAED patterns are observed in the HRTEM image (Figure 2g) and SAED patterns (Figure 2h) respectively. Detailed microstructure analysis of the N-C materials by TEM imaging is provided in an earlier publication 8 .

Open Access Article. Published on 05 Novemba 2025. Downloaded on 11/11/2025 06:10:41

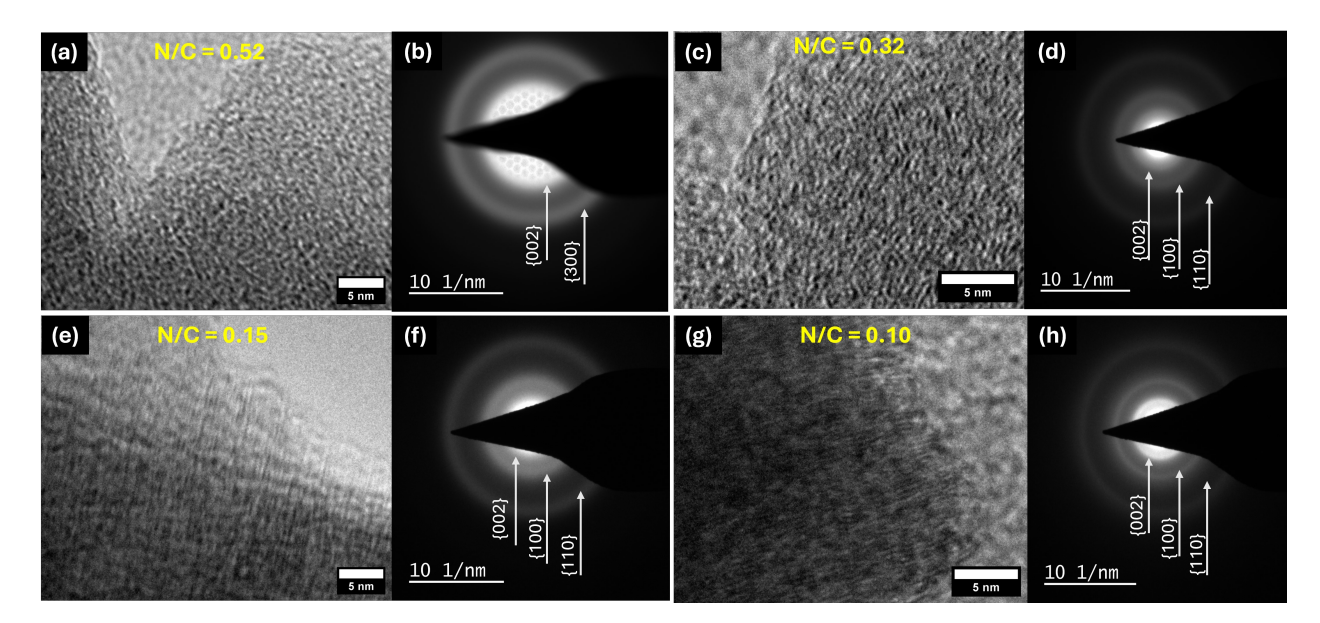


Figure 2: (a,c,e,g) HRTEM micrographs and (b,d,f,h) SAED patterns of N-C materials with N/C ratio of 0.52, 0.32, 0.15 and 0.10 respectively

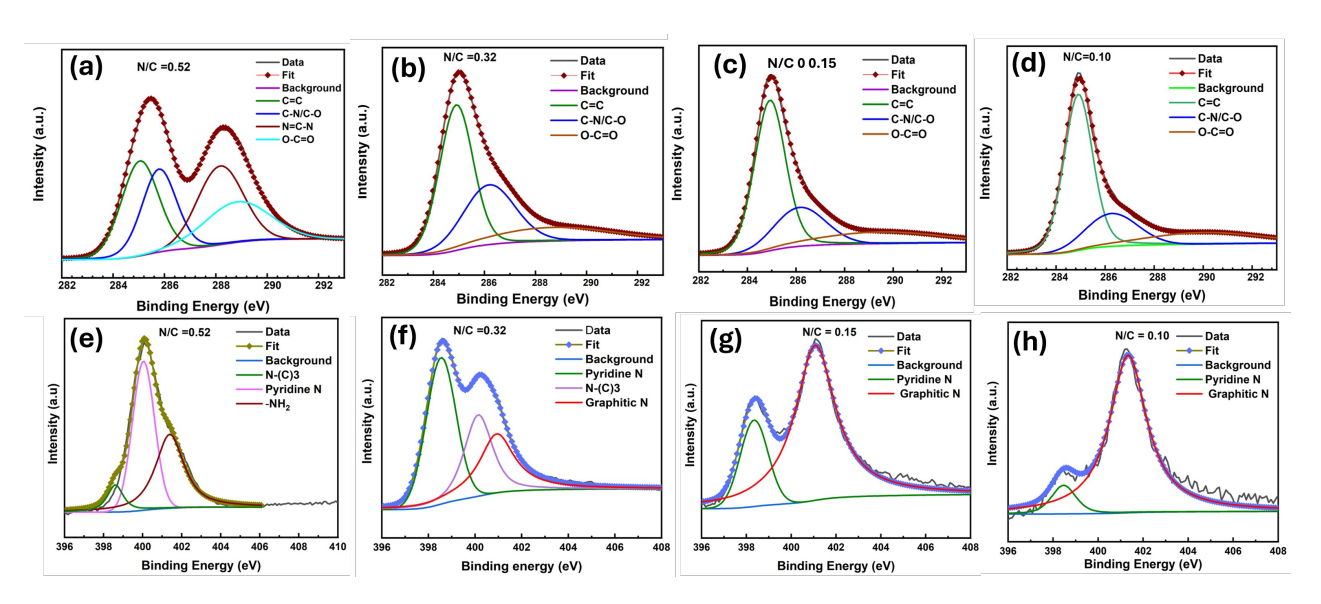


Figure 3: (a-d) C_{1s} spectra fit and (e-h) N_{1s} spectra fit of N-C materials with N/C ratio of 0.52, 0.32, 0.15 and 0.10.

Surface elemental composition and functional groups of N-C materials confirmed by XPS are provided in Figure 3a-d. The XPS survey spectrum is available in the SI (Figure S1). Based on the C_{1s} spectra, the fitted peaks for the material with N/C = 0.52 (Figure 3c) correspond to C=C (285.0 eV \pm 0.2), C-N/C-O (285.9 eV \pm 0.2), N=C-N (288.3 eV \pm 0.1),

and O=C-O (288.8 \pm 0.2 eV). For material with N/C = 0.32 (Figure 3b), 0.15 (Figure 3c), and 0.10 (Figure 3d), the C_{1s} peak fits indicate the presence of C=C, C-N/C-O, and O=C-O species.

Table 1: Results from the characterization of N-C materials featuring different N/C ratios.

Sample code	N/C (atomic ratio)	d ₀₀₂ (nm)	$\mathbf{I}_D/\mathbf{I}_G$	L_a (nm)	$egin{array}{c} \sigma(imes 10^{-6} \ { m S/cm}) \end{array}$	XPS (atomic %)	CHNS ⁸ (weight %)	Contact angle (°)
$N-C_2$	0.52	0.328	1.12	17.10	3	C(57.74),	C(37),	33±1
		± 0.002	± 0.01	± 1.5	± 1	N(17.77),	N(24.6),	
						O(24.49)	H(3.78)	
							O(36.16)	
$N-C_6$	0.32	0.349	1.19	16.14	12	C(75.30),	C(61.53),	38±1
		± 0.002	± 0.05	± 1.5	± 3	N(16.99),	N(25.95),	
						O(9.81)	H(2.93)	
							O(12.58)	
$N-C_9$	0.15	0.342	1.10	17.30	685	C(86.88),	C(79.85),	56±1
		± 0.005	± 0.02	± 1.3	± 26	N(10.76),	N(13.99),	
						O(2.47)	H(1.74)	
							O(4.91)	
$N-C_{13}$	0.10	0.338	1.01	19.03	1099	C(95.01),	C(85.5),	81±2
		± 0.004	± 0.04	± 1.7	± 49	N(3.78),	N(10),	
						O(1.31)	H(1)	
						· 	O(3.5)	

The results from the N_2 adsorption studies indicate that the material with N/C = 0.15exhibit the largest BET surface area among the four materials and the smallest average pore size (see Table 2 and figure S3 in the SI). This could attributed to the fact that at this N/C ratio (T = 900 °C), the N-C material fully transitions from g-CN (N/C = 0.52) to a graphitic material with pyridine and graphitic N in it ⁸. The smaller crystallite size and the presence of pyridine N in higher concentration is responsible for its higher surface area and lower pore size distribution compared to N/C = 0.10 (T = 1300 °C).

The different nitrogen species present on the material surfaces provide structural insights at specific N/C ratios. The three types of nitrogen species, identified from their N_{1s} spectra fit, are: N-(C)3 (400.3 eV \pm 0.1), pyridinic N (398.6 eV \pm 0.2), and graphitic N (401.2 \pm 0.2 eV). For N/C = 0.52, the fitted peaks include N-(C)3 species, representing N atoms bridging two triazine/hexagonal rings; pyridinic N, where N atoms alternate with C atoms

Table 2: Results from the adsorption studies of N-C materials featuring different N/C ratios.

Sample code	N/C (atomic ratio)	$\begin{array}{c} {\rm BET~surface~area} \\ {\rm (m^2/g)} \end{array}$	$egin{array}{ll} ext{Pore} & ext{volume} \ (ext{m}^3/ ext{g}) & \end{array}$	ime Average pore di- ameter (nm)
$N-C_2$	0.52	19.82 ± 1	0.12 ± 0.03	30.11 ± 1.3
N-C ₆	0.32	95.53 ± 3	0.35 ± 0.05	21.33±1
N-C ₉	0.15	132.07 ± 6	$0.42 {\pm} 0.02$	8.50 ± 0.5
$N-C_{13}$	0.10	21.05 ± 1.5	0.11 ± 0.01	$22.62 {\pm} 0.9$

in hexagons; and C-N species, attributed to surface amine groups (See Figure 3e). At N/C = 0.32 (See Figure 3f), pyridinic N, N-(C)3, and graphitic N species are observed. For N/C = 0.15 (See Figure 3g) and N/C = 0.10 (See Figure 3h), only pyridinic N and graphitic N species are identified from the peak fits. The proportions of these nitrogen species are detailed in the SI (Figure S2), from which the ratio of pyridinic N to graphitic N is calculated.

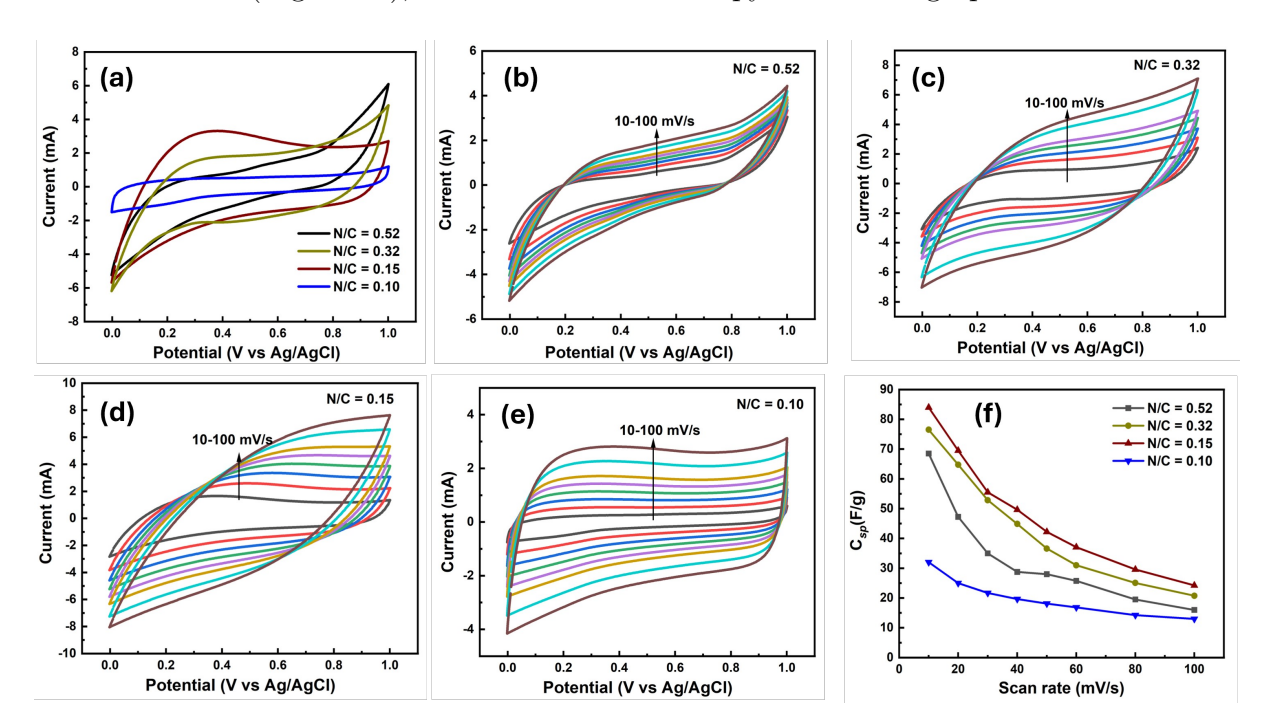


Figure 4: (a) Comparative cyclic voltammograms of N-C materials with N/C ratio of 0.52, 0.32, 0.15 and 0.10. Cyclic voltammograms at different scan rates for N-C materials with N/C ratio of (b) 0.52, (c) 0.32, (d) 0.15, and (e) 0.10. (f), specific capacitance vs scan rate plot for N-C materials with N/C ratio of 0.52, 0.32, 0.15 and 0.10.

A comparison of the cyclic voltammograms of the N-C materials within a voltage window of 0 to 1 V is depicted in Figure 4a. As shown, the CVs of N-C₂ (N/C = 0.52), N-C₆ (N/C =

0.32), N-C₉(N/C = 0.15) and N-C₁₃ (N/C = 0.10) at a scan rate of 10 mV/s exhibit a quasirectangular shape, indicating pseudocapacitive behavior of all the materials³⁴. The specific capacitance (C_s) calculated from the cyclic voltammograms (Figure 4a) using Equation 2 are 69, 78, 81 and 34 F/g for N-C₂, N-C₆, N-C₉ and N-C₁₃ respectively. The area under the CV curves is highest for N-C₉ at N/C ratio of 0.15, indicating its high electrochemically active surface area, hence high capacitance.

Nitrogen incorporation into the carbon network enhances electron donor properties, improving electron transfer kinetics at the electrode/electrolyte interface, enabling reversible redox reactions, and thereby contributing to pseudocapacitance in otherwise EDLC-type carbon-based materials²⁸. The extent of pseudocapacitance is also influenced by the chemical nature and type of bonding of nitrogen in the N-C systems, such as whether it is part of a compound (like g-CN) or present as defects in carbon. The quasi-rectangular shape of the cyclic voltammograms becomes more pronounced with decreasing nitrogen content, as N/C ratio reduces from 0.52 (for N-C₂) to 0.15 (N-C₉). Notably, it is N-C₉ (N/C ratio 0.15), and not N-C₁₃ (N/C = 0.10) that displays the most pronounced quasi-rectangular CV profile, signaling a reverse transition from pseudocapacitive to EDLC behavior as the N/C ratio further decreases.

Interestingly, we found that an increase in N content does not directly correlate with a higher capacitance. The capacitive performance of N-C systems is also strongly influenced by their electrical conductivity and nitrogen configuration. For crystalline g-CN with N/C ratio of 1.33, N is present alternatively with carbon on hexagonal rings and therefore the electron density is balanced. Here, nitrogen does not contribute to reversible redox reactions, which are essential for pseudocapacitance. Therefore, the supercapacitors made of pure g-CN are essentially of EDLC type 40 . However, in nitrogen-deficient g-CN systems (such as N-C₂, N/C = 0.52), the electron density is more shifted towards N atoms, and N atoms actively participate in redox reactions promoting pseudocapacitance 12 . In carbon systems with N atoms present as defects (as in the case of N-C₆, N-C₉, and N-C₁₃), the N

atoms more actively participate in reversible-redox reactions due to polarity shift between N and C atoms. These polarised atoms in a carbon material facilitate electrolyte ion diffusion and adsorption, promoting pseudocapacitance⁴¹. Additionally, the conductive carbon network reduces resistance at the electrode/ electrolyte interface, thereby enhancing the overall capacitance²⁵.

The capacitance of N-containing carbon also depends on the configuration of N, such as pyrrolic N, pyridine N or graphitic N present in the material 42 . The area under the cyclic voltammograms is highest for N-C₉ (N/C = 0.15), which benefits from a balance between surface area, electrical conductivity, wettability, and pyridine N content, all key characteristics of effective energy storage materials 43 . The reverse transition of the capacitive behavior from pseudo to EDLC for N-C₁₃ can be attributed to a lower fraction of pyridine N species 44,45 (See Figure SI1). CV measurements at different scan rates for the N-C systems are shown in Figure 4b-e. The C_s calculated from these cyclic voltammograms using Equation 2 at different scan rates are provided in Figure 4f. Even at higher scan rates, the cyclic voltammograms remain consistent for all N-C systems, with an increase in current response, likely due to an increase in areal capacitance.

To quantify the fraction of EDLC and faradaic reactions to the overall specific capacitance of each N-C materials, the Trasatti methodology was employed 42 . An initial scan was carried out at rates ranging from 10 mV/s to 100 mV/s to obtain the cyclic voltammograms (CVs) of each specimen. Following this data acquisition phase, the corresponding gravimetric specific capacitance (C_{sp}) was calculated using the formula presented in Equation 2.In this expression, A denotes the area enclosed by the CV curve, while m, v, and δ V represent the mass of the material in grams, the scan rate in mV/s, and the potential window in volts, respectively. The gravimetric capacitances, expressed as C_{sp}^{-1} , were plotted against the square root of the scan rates, denoted as $v^{0.5}$. This was performed with the expectation that a linear relationship between these variables would be revealed, under the assumption

of semi-infinite ion diffusion. The observed correlations can be described using Equation 3 and Equation 4.

$$C_{sp} = \frac{A}{2mv\delta v} \tag{2}$$

$$C_{sp}^{-1} = kv^{0.5} + C_T^{-1} (3)$$

$$C_{sp} = kv^{-0.5} + C_{EDLC} (4)$$

Here C_{sp} refers to the experimentally determined gravimetric capacitance, v corresponds to the scan rate, and C_T and C_{EDLC} represent the total capacitance and the electrical double-layer capacitance, respectively. By performing a linear fit on the plot and extrapolating the line to the y-axis, the maximum value of the EDLC is determined. The maximum capacitance from faradaic reactions is then obtained by subtracting the value of C_{EDLC} from the total capacitance C_T . The results derived through this method are presented in Table 3. It is found that the material with N/C ratio of 0.15 exhibits the highest value of capacitance contribution from faradaic reactions. Additionally, the rate capability index (b) is critical for understanding the charge storage mechanism in supercapacitors. The b values for the N-C materials are provided in Table 3 and the values lies between 0.5 and 1. This indicate a hybrid charge storage mechanism indicative of pseudocapacitive materials, with N/C =0.10 exhibitting the highest rate capability among the four materials.

To further study the effect of N/C ratio on the supercapacitor perfromance of the N-C systems, GCD measurements were conducted at various current densities, as depicted in (Figure 5 a) through f. (Figure 4 a) illustrates the comparative GCD curves of the four N-C materials at a current density of 1 A/g. The GCD curves exhibited a nearly triangular shape (Figure 4 a), with a non-linear discharge pattern characteristic of pseudocapacitive behavior. This observed charge-discharge pattern aligns with the behavior seen in cyclic

Table 3: Contributions of EDLC capacitance and faradaic capacitance to the overall capacitance of N–C materials. In the sample codes, the subscripted number denotes the preparation temperature/ 100.

Sample code	N/C (atomic ratio)	$rac{ ext{EDLC}}{(ext{F/g})}$	$\begin{array}{c} \text{Faradaic} \\ \text{capacitance} \\ (\text{F/g}) \end{array}$	% EDLC	% Faradaic capacitance	rate per- formance index,b
N-C ₂	0.52	20.90	42.75	32.84	67.16	0.6833
N-C ₆	0.32	24.40	52.15	31.97	68.03	0.6696
N-C ₉	0.15	25.99	59.15	30,52	69,47	0.7284
$N-C_{13}$	0.10	17.15	12.30	58.62	41.38	0.8412

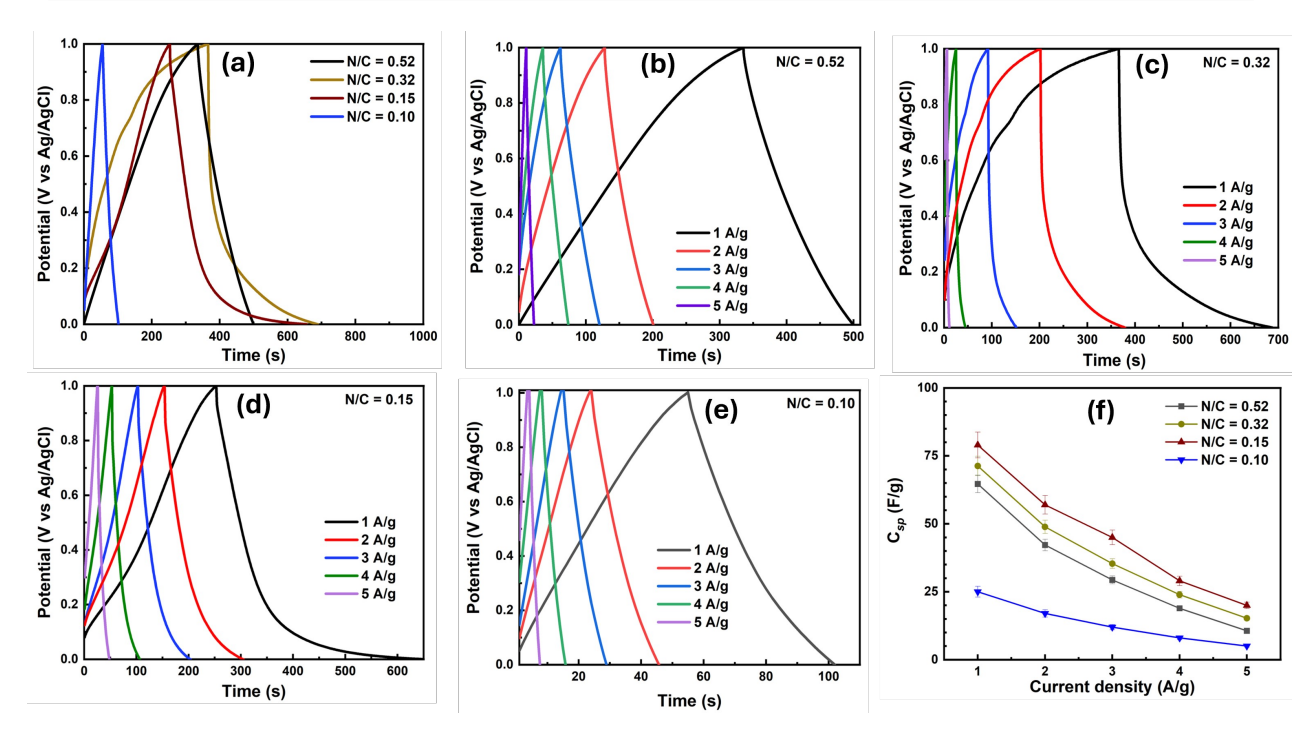


Figure 5: (a) Comparative galvanostatic charge-discharge curves of N-C materials with N/C ratio of 0.52, 0.32, 0.15 and 0.10 at 1 A/g. Galvanostatic charge-discharge curves at different current densities for N-C materials with N/C ratios of (b) 0.52, (c) 0.32, (d) 0.15, and (e) 0.10. (f) Specific capacitance vs current density plot for N-C materials with N/C ratios of 0.52, 0.32, 0.15 and 0.10.

voltammograms, further confirming the pseudocapacitive nature. C_{sp} values for the N-C materials at current density of 1 A/g calculated using the formula provided in Equation 5 are 64.67 ± 2.5 , 71.29 ± 3.2 , 79.25 ± 3.8 and 25.55 ± 1.9 F/g for N/C = 0.52, N/C = 0.32, N/C = 0.15 and N/C = 0.10 respectively. The GCD at different current densities for the N-C systems are presented in (Figure 4b-e), revealing that the non-linear discharge pattern are maintained even at higher current densities. The plot of C_{sp} derived from these GCD curves

Journal of Materials Chemistry A Accepted Manuscript

(Figure 5 b-e) at different current densities are provided in Figure 5f). The corresponding areal and volumetric capacitance values corresponding to the gravimetric capacitances at different current densities are provided in Table SI of the SI.

$$C_{sp} = \frac{I\delta t}{m\delta v} \tag{5}$$

Where, I is the current applied, δt is the discharge time, m is the mass loading, and δV represents the potential window.

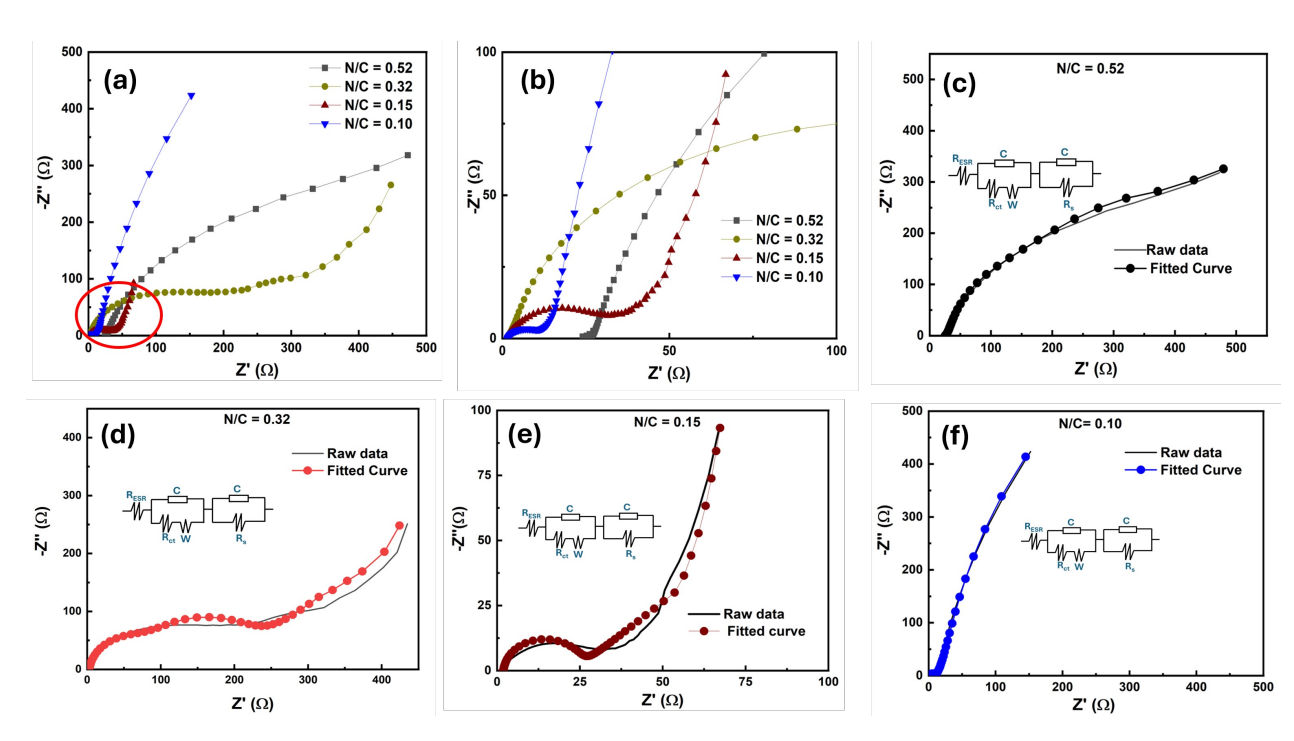


Figure 6: (a) Comparative Nyquist plots and (b) enlarged Nyquist plot of the red encircled region in (a), obtained from electrochemical impedance spectroscopy for N-C materials with N/C ratios of 0.52, 0.32, 0.15 and 0.10.(c-f) Fitted Nyquist plots with equivaent circuit diagrams for (c) N/C = 0.52, (d) N/C = 0.32, (e) N/C = 0.15 and (f) (c) N/C = 0.10.

The Nyquist plots of N/C = 0.52 (Figure 6 a and c), also see enlarged Nyquist plot in (Figure 6 b) exhibit a linear trend without a noticeable semicircle region, indicating a low charge transfer resistance (R_{ct}) at the electrode/ electrolyte interface for the N-C material. The R_{ct} values can be correlated to the porous nature of these materials, indicating that N/C = 0.52 has a lower fraction of meso and micro pores. The presence of a semicircle in the high-frequency region in the Nyquist plots of N/C = 0.32, N/C = 0.15, and N/C = 0.10 (see Figure 6b, also see Figure 6d, e and f) indicate the presence of smaller sized pores, indicating their high surface area. The R_{ct} values are 75.9, 12.8 and 5.9 Ω respectively for N/C = 0.32, N/C = 0.15, and N/C = 0.10 respectively. The equivalent series resistance (ESR) values were calculated to be 23.58, 1.52, 1.59, and 1.06 Ω for N/C = 0.52, N/C = 0.32, N/C = 0.15, and N/C = 0.10 respectively. In the high frequency region, the Nyquist plot of N-C₆ and N-C₉ resemble that of pseudocapacitive carbon materials while that of N/C = 0.10 resembles the Nyquist plot of EDLC-type carbon materials ⁴⁶. Evidently, N/C = 0.15 exhibit the overall lowest resistance, indicative of its high capacitance. Individual fitted Nyquist plots of the four N-C materials with their equivalent circuit diagrams are provided in Figure 6c-f. Additionally, N/C = 0.52, 0.32 and 0.15 exhibitted phase angles between -45 to 70 °indicating pseucapacitive behavior and in the case of N/C = 0.10, phase angles at lower frequency indicated EDLC dominant behavior (see Figure S4).

The long-term stability of the N-C materials was evaluated through GCD cycling over 2500 cycles at a current density of 25 A/g (refer to Figure 7(a-d). For the sample with N/C = 0.52 (Figure 7a), the capacitance retention increased to 102 % around the 1000^{th} cycle, after which it began to decline, reaching 94.30 % at the end of 2500 cycles. The Coulombic efficiency remained steady at 55.50 %. In the case of N/C = 0.32 (Figure 7b), the capacitance consistently increased with cycling, achieving a retention of 105.2 % after 2500 GCD cycles, with the Coulombic efficiency stably maintained at 67.10 %. For N/C = 0.15 and 0.10 (Figure 7c and d), capacitance retention remained constant (100 %) up to 1500 cycles, followed by a gradual decline. Final capacitance retentions of 96.10 % and 98.50 % were observed for N/C = 0.15 and 0.10, respectively. At these lower N/C ratios, the N-C materials demonstrated high Coulombic efficiencies of 98.90 % at the end of 2500 cycles. A high coulombic efficiency of 99.98 % is maintained even at low current density of 1A/g for

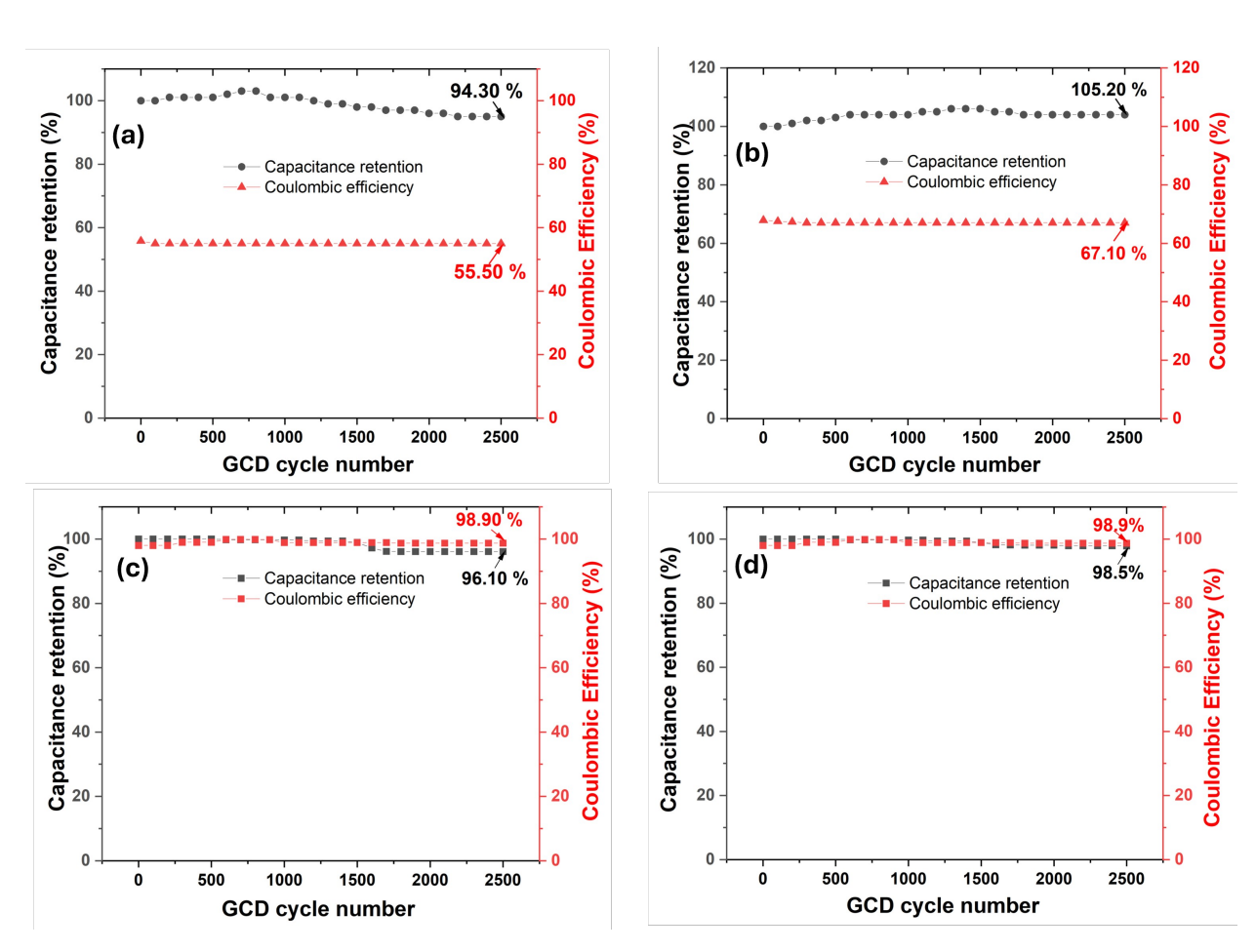


Figure 7: Capacitance retention and coulombic efficiency plots measured via GCD for 2500 cycles for N-C materials (a) N/C = 0.52, (b) N/C = 0.32, (c) N/C = 0.15 and (d) N/C = 0.10

10k cycles in the case of N/C = 0.15 (see Figure S5).

The variation in long-term stability results of the N-C materials can be attributed to differences in the N/C ratios and the distinct configurations of nitrogen within the graphitic framework. For samples with N/C = 0.52 and 0.32, which possess a high pyridine content, the observed increase in capacitance after several hundred GCD cycles is due to electrochemical activation of the electrode⁴⁷. With continued GCD cycling, the electrolyte penetrates deeper into the electrode, enabling access to active sites, particularly pyridine N, that contribute to pseudocapacitance, increasing the overall capacitance. However, this elevated pyridine N content⁴⁸, along with increased oxygen levels, promotes parasitic side reactions such as the oxygen evolution reaction (OER) at the electrode/electrolyte interface of materials with N/C

= 0.52 and 0.32, accounting for the lower coulombic efficiency. As the N/C ratio decreases, the coulombic efficiency improves due to the reduced presence of pyridine N, which in turn limits parasitic reactions like OER. Furthermore, at lower N/C ratios (associated with higher heat-treatment temperatures), the oxygen content in the materials is also reduced (see XPS data in Table 1 and Figure S1). Consequently, the lower coulombic efficiencies observed in high N/C ratio materials can be attributed to parasitic reactions involving both pyridine N and oxygen species.

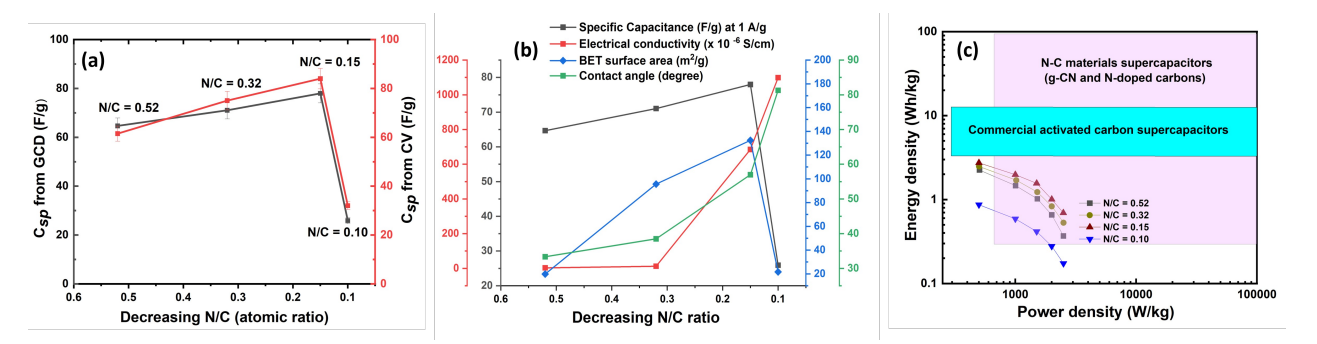


Figure 8: (a) Relation of N/C atomic ratio of the N-C materials with specific capacitance deduced from cyclic voltammetry at 10 mV/s and galvanostatic charge-discharge tests at 1 A/g from three-electrode study, (c) relation of N/C ratio with other material properties which influence the capacitance in N-C materials, (c) Comparative ragone plot of the N-C materials.

In Figure 8a, the variation of C_{sp} calculated from the CV and GCD plots at 10 mV/s and 1 A/g for different N/C ratios are shown. The trend of capacitance is similar for the values calculated from CV and GCD, indicating that the N-C material at N/C = 0.15 exhibits the highest capacitance. All electrochemical data allude to the fact that the supercapacitive performance of N-C materials, in terms of their long time stability and coulombic efficiencies, peaks at an N/C ratio of around 0.15, particularly when the ratio of pyridine N (N6) to graphitic N (NQ) is 0.33 (see Table 1). At this N6/NQ ratio, the N-C material exists as a disordered carbon where the sp^2 carbon sheets in the graphitic crystallites have N6 and NQ atoms present as defects. In such a disordered carbon, N6 provides active sites for reversible redox reactions and contributes to a high surface area, while NQ enhances electrical

conductivity and limiting the parasitic side reactions. Both nitrogen species improve wetting characteristics in the otherwise hydrophobic carbon material. This combination creates an optimal balance between conductivity, wettability and surface area, leading to superior electrochemical performance (see Figure 8b). Further decreasing the N/C ratio through higher-temperature heat treatment is expected to reduce the capacitance, with the resulting supercapacitor behavior dominated by EDLC. This treatment likely converts all pyridinic nitrogen into graphitic nitrogen, making the material more graphitic and eliminating active sites necessary for promoting pseudocapacitance.

In Figure 8c, the ragone plot of the N-C materials compared to reported N-C materials and commercial activated carbon devices are shown. Device level (symmetric supercapacitor) capacitance of the N-C materials were calculated from the three electrode capacitance using the Equation 6 (data provided in the SI, Figure S6) from which the Energy density, E (Wh/kg) and power density, P (W/kg) was calculated using Equation 7 and Equation 8 respectively. In these equantions, C is the capacitance, V is the voltage window and t is the discharge time in seconds. The N-C materials reported in this work fall in the range of supercapacitive N-C materials ^{12,28} in the ragone plot and their E and P values are slightly lower than that of commercial activated carbon supercapacitors ⁴⁹. Further activation of the N-C materials by KOH treatment/CO₂ activation can enhance their device-level performance. Three-electrode supercapacitor study of the N-C material with N/C= 0.15 in 1 M TEABF₄/AN (see Figure S7 in the SI) confirm that the material is stable in organic electrolytes as well. This suggests that exploring the device-level supercapacitor performance of such N-C materials in various electrolyte systems could pave the way for their application in powering next-generation wearable electronic devices.

$$C_{sp}(device) = \frac{C_{sp}(electrode)}{4} \tag{6}$$

$$E = \frac{1}{2} \times CV^2 \times \frac{1}{3.6} \tag{7}$$

$$P = \frac{E \times 3600}{t} \tag{8}$$

Conclusion

In conclusion, we investigated the effect of nitrogen content on the supercapacitor performance of N-C materials with N/C ratios ranging from 0.52 to 0.10. Such materials are typically prepared by thermal denitrogenation of g-CN, and are devoid of pyrrolic N. The presence of pyridinic N plays a key role in enhancing capacitance, with an optimal pyridinic to graphitic N ratio of 0.33. It was found that for this class of materials, an increase in the N/C ratio does not directly correlate to an increase in capacitance. Supercapacitor performance depends on the crystal structure at that particular N/C ratio. The N/C ratio determines whether the material exists as g-CN or as a carbon with N incorporated in defect sites. These structural disparity at varying N/C ratios impacts the key physicochemical properties like surface area, conductivity and wettability, which in turn dictate the electrochemical behavior. The highest capacitance recorded was $79.25 \pm 3.8 \text{ F/g}$ at 1 A/g for the material with N/C = 0.15.

This work establishes a foundation for understanding the role of N/C ratios in N-C materials derived from g-CN precursors. Our findings can serve as useful guidelines for optimizing the N content or N/C ratio in electrode materials designed for high-performance supercapacitors. N-C materials are expected to provide a significant boost to the existing supercapacitor technology, facilitating cheaper and greener alternatives to elemental carbon. The results reported here enable researchers to evaluate the potential of their N-C material in energy applications simply by conducting elemental analysis and XPS. Future work can focus on studying the impact of O content and the variation in O species on supercapacitor performance.

Author contribution

M.D.: conceptualization, design, data analysis, and drafting of the manuscript, J.S.: Data acquisition and drafting of the manuscript and S.S.: Manuscript review & editing, funding

Open Access Article. Published on 05 Novemba 2025. Downloaded on 11/11/2025 06:10:41

acquisition, supervision.

Conflicts of interest

The authors declare that there are no conflict(s) of interest.

Data availability

All data supporting the findings of this study are included in the paper and its supporting information. Source data are available from the corresponding author (S.S.) upon reasonable request.

Acknowledgments

M.D. and J.S. would like to thank the Ministry of Education, Government of India, for their doctoral fellowships. Authors acknowledge the Advanced Materials and Research Center and the Center for Design and Fabrication of Electronic Devices, IIT Mandi, for providing access to characterization facilities.

References

- (1) Inagaki, M.; Toyoda, M.; Soneda, Y.; Morishita, T. Nitrogen-doped carbon materials. Carbon 2018, 132, 104–140.
- (2) Guo, H.; Sun, T.; Yin, Q.; Li, X.; Chen, Z.; Ma, X. Heteroatom-doped lignin-derived carbon material: performance and application. Sustainable Energy & Fuels 2024, 8, 1369–1388.
- (3) Liu, L.; Zhang, W.; Lu, B.; Cheng, Z.; Cao, H.; Li, J.; Fan, Z.; An, X. Controllable heteroatoms doped electrodes engineered by biomass based carbon for advanced supercapacitors: A review. *Biomass and Bioenergy* **2024**, *186*, 107265.
- (4) Zheng, Y.; Li, C.; Liu, J.; Wei, J.; Ye, H. Diamond with nitrogen: states, control, and applications. *Functional Diamond* **2021**, *1*, 63–82.
- (5) Zhou, H.; Zhang, X.; Zhang, X.; Yuan, F.; Wang, X.; Yan, S.; Wang, J.; Li, C.; Sun, Z. N-doped microcrystalline graphite for boosting peroxymonosulfate activation with highly efficient degradation of bisphenol A. Carbon 2024, 216, 118579.
- (6) Mainali, K.; Mood, S. H.; Pelaez-Samaniego, M. R.; Sierra-Jimenez, V.; Garcia-Perez, M. Production and applications of N-doped carbons from bioresources: A review. Catalysis Today 2023, 423, 114248.
- (7) Jeon, I.; Noh, H.; Baek, J. Nitrogen-Doped Carbon Nanomaterials: Synthesis, Characteristics and Applications. *Chemistry An Asian Journal* **2020**, *15*, 2282–2293.
- (8) Devi, M.; Pandey, P.; Sharma, S. Crystalline–disordered–crystalline transition in nitrogen–carbon materials. *Journal of Applied Physics* **2025**, *137*, 025104.
- (9) Sharma, S.; Zorzi, S.; Cristiglio, V.; Schweins, R.; Mondelli, C. Quantification of Buck-minsterfullerene (C60) in non-graphitizing carbon and a microstructural comparison of

- graphitizing and non-graphitizing carbon via Small Angle Neutron Scattering. *Carbon* **2022**, *189*, 362–368.
- (10) Kaushal, S.; Andrews, J. A review on the nitrogenated carbon materials and their electrochemical performance for energy storage applications. *International Journal of Hydrogen Energy* **2025**, *100*, 1231–1245.
- (11) Jiang, Q.; Cai, Y.; Sang, X.; Zhang, Q.; Ma, J.; Chen, X. Nitrogen-Doped Carbon Materials As Supercapacitor Electrodes: A Mini Review. *Energy & Fuels* **2024**, *38*, 10542–10559.
- (12) Devi, M.; Upadhyay, S.; Mir, R. A.; Kumar, N.; Sharma, S. Synthetic waste derived graphitic carbon nitride (g-CN) and g-CN/carbon hybrid for supercapacitors. *Journal of Energy Storage* **2023**, *73*, 109067.
- (13) Zhao, J.; Lai, H.; Lyu, Z.; Jiang, Y.; Xie, K.; Wang, X.; Wu, Q.; Yang, L.; Jin, Z.; Ma, Y.; Liu, J.; Hu, Z. Hydrophilic Hierarchical Nitrogen-Doped Carbon Nanocages for Ultrahigh Supercapacitive Performance. Advanced Materials 2015, 27, 3541–3545.
- (14) Adeniji, A.; Beda, A.; Fioux, P.; Matei Ghimbeu, C. Engineering nitrogen-doped porous carbon positive electrodes for high-performance sodium-ion capacitors: the critical role of porosity, structure and surface functionalities. J. Mater. Chem. A 2025, 13, 14896– 14914.
- (15) Prieto, M.; Ellis, G. J.; Budarin, V.; Morales, E.; Naffakh, M.; Shuttleworth, P. S. Understanding pore size relation in cellulose-derived, nitrogen-doped, hydrothermal carbons for improved supercapacitor performance. J. Mater. Chem. A 2024, 12, 29698–29707.
- (16) Zhu, G.; Ma, L.; Lv, H.; Hu, Y.; Chen, T.; Chen, R.; Liang, J.; Wang, X.; Wang, Y.; Yan, C.; Tie, Z.; Jin, Z.; Liu, J. Pine needle-derived microporous nitrogen-doped carbon

- (17) Zhu, G.; Chen, T.; Wang, L.; Ma, L.; Hu, Y.; Chen, R.; Wang, Y.; Wang, C.; Yan, W.; Tie, Z.; Liu, J.; Jin, Z. High energy density hybrid lithium-ion capacitor enabled by Co3ZnC@N-doped carbon nanopolyhedra anode and microporous carbon cathode. Energy Storage Materials 2018, 14, 246–252.
- (18) Yesuraj, J.; Naveenkumar, P.; Maniyazagan, M.; Yang, H.-W.; Kim, S.-J.; Kim, K. Fabrication of N-doped carbon coated CoFeS2 anchored rGO nanosheet composites: a twin carbon design for Li-ion storage and high energy density supercapacitor applications.

 J. Mater. Chem. A 2025, 13, 21830–21846.

- (19) Inagaki, M.; Tsumura, T.; Kinumoto, T.; Toyoda, M. Graphitic carbon nitrides (g-C3N4) with comparative discussion to carbon materials. *Carbon* **2019**, *141*, 580–607.
- (20) Miao, J.; Geng, W.; Alvarez, P. J. J.; Long, M. 2D N-Doped Porous Carbon Derived from Polydopamine-Coated Graphitic Carbon Nitride for Efficient Nonradical Activation of Peroxymonosulfate. *Environmental Science & Technology* 2020, 54, 8473–8481, PMID: 32511905.
- (21) Chen, H.; Sun, F.; Wang, J.; Li, W.; Qiao, W.; Ling, L.; Long, D. Nitrogen Doping Effects on the Physical and Chemical Properties of Mesoporous Carbons. *The Journal* of Physical Chemistry C 2013, 117, 8318–8328.
- (22) Wiggins-Camacho, J. D.; Stevenson, K. J. Effect of Nitrogen Concentration on Capacitance, Density of States, Electronic Conductivity, and Morphology of N-Doped Carbon Nanotube Electrodes. The Journal of Physical Chemistry C 2009, 113, 19082–19090.
- (23) Ganesan, R.; Xavier, J. R. Fabrication of polythiophene/graphitic carbon nitride/V2O5 nanocomposite for high-performance supercapacitor electrode. *Materials Science and Engineering: B* 2024, 300, 117101.

- (24) Chu, Q.; Chen, Z.; Cui, C.; Zhang, Y.; Li, X.; Liu, G.; Yang, H.; Cui, Y.; Li, Y.; Liu, Q. Pyrrolic-N/C = O cooperative assisted in hollow porous carbon with ultra-high electrochemical performance for Zn-ion hybrid supercapacitors. *Applied Surface Science* **2024**, *654*, 159461.
- (25) Xiao, B.-H.; Lin, R.-T.; Xiao, K.; Liu, Z.-Q. A highly compressible, nitrogen doped carbon foam based all pseudo-capacitance asymmetric supercapacitors. *Journal of Power Sources* **2022**, *530*, 231307.
- (26) Hulicova-Jurcakova, D.; Seredych, M.; Lu, G. Q.; Bandosz, T. J. Combined Effect of Nitrogen- and Oxygen-Containing Functional Groups of Microporous Activated Carbon on its Electrochemical Performance in Supercapacitors. Advanced Functional Materials 2009, 19, 438–447.
- (27) Lota, G.; Grzyb, B.; Machnikowska, H.; Machnikowski, J.; Frackowiak, E. Effect of nitrogen in carbon electrode on the supercapacitor performance. *Chemical Physics Letters* **2005**, 404, 53–58.
- (28) Deng, Y.; Xie, Y.; Zou, K.; Ji, X. Review on recent advances in nitrogen-doped carbons: preparations and applications in supercapacitors. *Journal of Materials Chemistry A* **2016**, 4, 1144–1173.
- (29) Gao, Y.; Li, T.; Zhu, Y.; Chen, Z.; Liang, J.; Zeng, Q.; Lyu, L.; Hu, C. Highly nitrogen-doped porous carbon transformed from graphitic carbon nitride for efficient metal-free catalysis. *Journal of Hazardous Materials* **2020**, *393*, 121280.
- (30) Xiong, K.; Liu, Z.; Ren, L.; Li, D.; Dong, K.; Yang, L.; Zhang, X. N and O dual-doped porous carbon transformed from graphitic carbon nitride as a peroxymonosulfate activator for tetracycline hydrochloride degradation. New J. Chem. 2025, 49, 855–864.
- (31) Krüner, B.; Schreiber, A.; Tolosa, A.; Quade, A.; Badaczewski, F.; Pfaff, T.;

- (32) Jangra, R.; Mahendia, P.; Karakoti, M.; Sahoo, N.; Srivastava, A.; Sinha, O.; Clemons, T. D.; Deshpande, U.; Mahendia, S. ZnCl2-assisted conversion of nitrogen-containing biomass carbon from marigold flower: Toward highly porous activated nitrogen-doped carbon for low ESR and enhanced energy density supercapacitors. *Journal of Energy Storage* 2024, 75, 109728.
- (33) Cao, L.; Li, H.; Xu, Z.; Zhang, H.; Ding, L.; Wang, S.; Zhang, G.; Hou, H.; Xu, W.; Yang, F.; Jiang, S. Comparison of the heteroatoms-doped biomass-derived carbon prepared by one-step nitrogen-containing activator for high performance supercapacitor. *Diamond and Related Materials* **2021**, *114*, 108316.

- (34) Gogotsi, Y.; Penner, R. M. Energy Storage in Nanomaterials Capacitive, Pseudocapacitive, or Battery-like? *ACS Nano* **2018**, *12*, 2081–2083.
- (35) Andreyev, A.; Akaishi, M.; Golberg, D. Synthesis of nanocrystalline nitrogen-rich carbon nitride powders at high pressure. *Diamond and Related Materials* **2002**, *11*, 1885–1889.
- (36) Zinin, P. V.; Ming, L.-C.; Sharma, S. K.; Khabashesku, V. N.; Liu, X.; Hong, S.; Endo, S.; Acosta, T. Ultraviolet and near-infrared Raman spectroscopy of graphitic C3N4 phase. Chemical Physics Letters 2009, 472, 69–73.
- (37) Li, W.; Peng, D.; Huang, W.; Zhang, X.; Hou, Z.; Zhang, W.; Lin, B.; Xing, Z. Adjusting coherence length of expanded graphite by self-activation and its electrochemical implication in potassium ion battery. *Carbon* **2023**, *204*, 315–324.
- (38) Li, W.; Xiao, M.; Jiang, J.; Li, Y.; Zhang, X.; Li, S.; Lin, X.; Peng, D.; Or, S. W.; Sun, S.; Xing, Z. Co4N nanoparticles embedded in N-doped carbon pores: Advanced interlayer material for lithium-sulfur batteries. *Nano Energy* **2025**, *142*, 111140.

- (40) Chen, Q.; Zhao, Y.; Huang, X.; Chen, N.; Qu, L. Three-dimensional graphitic carbon nitride functionalized graphene-based high-performance supercapacitors. *Journal of Materials Chemistry A* **2015**, *3*, 6761–6766.
- (41) Zhu, W.; Shen, D.; Xie, H. Combination of chemical activation and nitrogen doping toward hierarchical porous carbon from houttuynia cordata for supercapacitors. *Journal of Energy Storage* **2023**, *60*, 106595.
- (42) Zhu, W.; Shen, D.; Xie, H. Effect of Heteroatoms on Pseudocapacitance for N/O Codoped Porous Carbon in an Alkaline Aqueous Electrolyte. *Energy & Fuels* **2023**, *37*, 12467–12473.
- (43) Szubzda, B.; Szmaja, A.; Halama, A. Influence of structure and wettability of supercapacitor electrodes carbon materials on their electrochemical properties in water and organic solutions. *Electrochimica Acta* **2012**, *86*, 255–259, EREM 2011 + ISEE'Cap 2011 + EMRS 2011.
- (44) Lota, G.; Frackowiak, E. Pseudocapacitance Effects for Enhancement of Capacitor Performance. Fuel Cells 2010, 10, 848–855.
- (45) Lee, Y.-H.; Chang, K.-H.; Hu, C.-C. Differentiate the pseudocapacitance and double-layer capacitance contributions for nitrogen-doped reduced graphene oxide in acidic and alkaline electrolytes. *Journal of Power Sources* **2013**, *227*, 300–308.
- (46) Mei, B.-A.; Munteshari, O.; Lau, J.; Dunn, B.; Pilon, L. Physical Interpretations of Nyquist Plots for EDLC Electrodes and Devices. The Journal of Physical Chemistry C 2018, 122, 194–206.

- (47) Chen, D. R.; Adusei, P. K.; Chitranshi, M.; Fang, Y.; Johnson, K.; Schulz, M.; Shanov, V. Electrochemical activation to enhance the volumetric performance of carbon nanotube electrodes. *Applied Surface Science* **2021**, *541*, 148448.
- (48) Faisal, S. N.; Haque, E.; Noorbehesht, N.; Zhang, W.; Harris, A. T.; Church, T.; Minett, A. I. Pyridinic and graphitic nitrogen-rich graphene for high-performance supercapacitors and metal-free bifunctional electrocatalysts for ORR and OER. RSC Advances 2017, 7, 17950–17958.
- (49) Rajput, S.; Tyagi, V.; Sonika; Nayak, R.; Verma, S. K. Waste-Derived Activated Carbon for Supercapacitors: Current Trends and Future Prospects. *Energy Technology* 2025, 13, 2401977.

View Article Online DOI: 10.1039/D5TA06469D

Open Access Article. Published on 05 Novemba 2025. Downloaded on 11/11/2025 06:10:41. This article is licensed under a Creative Commons Attribution-NonCommercial 3.0 Unported Licence.

Data Availability Statement

All data supporting the findings of this study are included in the paper and its supporting information. Source data may be uploaded on a repository on acceptance of the manuscript.